Korean J. Chem. Eng., 39(1), 198-208 (2022)
DOI: 10.1007/s11814-021-0880-7

pISSN: 0256-1115
eISSN: 1975-7220

Adsorption capacity of sodium dodecyl sulfate activation okara for methylene blue on aqueous solution

Cailian Yu*, Bolin Li*, Kexin Zhang, Fen Li*, and Hong Yan*,†**

*School of Chemical and Environmental Engineering, Harbin University of Science and Technology, Harbin 150040, China
**Department of Natural Resourses of Suihua City, No.2 Xianghe Street, North Forth East Road, Bei Lin District, Suihua 152000, China

(*Received 27 January 2021 • Revised 19 March 2021 • Accepted 27 June 2021*)

Abstract−Agricultural waste okara (OA) was selected as a precursor to prepare low-cost adsorbent for the removal of methylene blue (MB). Sodium dodecyl sulfate (SDS), as a kind of anionic surfactant, was loaded onto okara (SOA) to achieve high adsorption ability. Scanning electron microscopy, Fourier transform infrared spectrometer and X-ray diffraction were investigated for the materials characterization. The effect of pH, contact time, initial concentration, adsorbent dose and ionic strength was determined to explore the adsorption properties. The adsorption kinetics, adsorption isotherms, cost analysis of adsorbent and adsorption mechanism were discussed. And the adsorption equilibrium data fitted well with Langmuir model, while the calculated maximum adsorption capacity was 238.10 mg g^{-1} for OA and 334.83 mg g^{-1} for SOA, respectively. The kinetics data followed the pseudo-second-order model. Thermodynamic parameters (ΔH^o, ΔG^o and ΔS^o) indicated the spontaneous and exothermal nature. This research reveals that SOA is an effective, low-cost and promising adsorbent on the adsorption of MB on aqueous solution.

Keywords: Adsorption, Dye, Okara, SDS, Agricultural Waste

INTRODUCTION

Dyes are widely used in many industries, such as paper, printing, food, plastics and leather. Every year, these industries produce more than 7×10^5 tons of dyes in China [1] and part of the untreated dye wastewater has flowed into rivers, lakes, and seas [2]. Dyes wastewater has caused a harmful effect on human and aquatic organism health due to its toxicity, refractory, and high chromaticity [3,4]. Among them, methylene blue (MB) is a well-known and hazardous typical cationic dye [5-7]. In recent years, many methods have been devoted to remove dye wastewater, such as photocatalysis [8], chemical oxidation, biological method and adsorption [9]. Among them, adsorption is the most effective method due to its high efficiency and stability [10,11]. However, though its excellent adsorption ability, activated carbon is not selected as a better adsorbent with its high cost [12]. Hence, to explore effective, low-cost and easily available biosorbent, agricultural waste has received more attention over the past few decades [13-15].

Okara is derived from tofu and soymilk production and so on, which is widely generated in Asian countries, especially in China. However, as a result of the production and processing of waste-soybean residue, the output is huge, about 20 million tons per year [16]. Okara also contains numerous nutrients, a small part of which are used in feed, but it is difficult to transport because of its corruption, and most of it is discarded directly, which results in a certain waste of resources and environmental problems. How to realize the reuse of okara has become a major environmental problem [17].

The proportion of common nutritional components per 100 g of dried okara is shown in the following Table 1. Several studies have indicated that okara can be used as a precursor for the removal of pollutants; for example, okara was used to remove Cd^{2+} and Zn^{2+} from aqueous solution [18]. The effects of contact time, solution pH, adsorbent dose and initial solution concentration were studied. As the results showed, the optimum was at Cd^{2+} solution pH 6.0 and Zn^{2+} solution pH 7.0, solution concentration 50 mg L^{-1}, adsorbent dose 10 g L^{-1} and contact time 12 h. Gao et al. utilized acid treated okara as a biosorbent to adsorb Acid Red (AR14) and Reactive Red 15 (RR15) solutions [19]. The experimental data at different concentration level was fitted well with Langmuir isotherm (100-300 mg L^{-1}) and Freundlich isotherm (300-500 mg L^{-1}); the obtained maximum adsorption capacity from Langmuir isotherm for AR14 and RR15 was 217.39 mg g^{-1} and 243.90 mg g^{-1}, respectively. Ye et al. studied epichlorohydrin and dimethylamine modified okara for the adsorption of acid fuchsin from kinetics and thermodynamics [20]. The results indicated the adsorption process followed the second-order kinetic model and was favored at high temperature. At the same time, thermodynamical study revealed that the adsorption process was spontaneous and endothermic. In this work, okara was used as a novel biosorbent for the removal of MB because of its low cost and easy availability. However, to the authors' knowledge, there are very few studies reported about the use of okara as a biosorbent for the MB adsorption previously. Recently, a new method has been adopted to enhance the adsorption ability by using a method of surfactant surface modification. Surfactants can be coated on the adsorbent surface to alter their properties. Hence, surfactants have been adopted to remove heavy mental ions

†To whom correspondence should be addressed.
E-mail: yanhong204821@aliyun.com

Table 1. General properties of okara

Materials	Water (%)	Protein (%)	Fat (%)	Ash (%)	Cellulose (%)	pH
OA	8.31	19.32	12.40	3.54	51.80	5.2

and other organic pollutants [21,22].

Sodium dodecyl sulfate (SDS) is a kind of nontoxic and anionic surfactant which is commonly used to enhance the solubility of organic pollutants. Some studies have shown that SDS promoted the removal of MB by anodic porous alumina, *Salacca zalacca* skin and activated carbon [23-25].

We expected that the loading of SDS would increase the adsorption capacity of OA to MB. Our study compared the adsorption capacity of okara (OA) and SDS-loaded okara (SOA), then revealed the mechanism of the reaction and the role of modification via a series of characterization methods. These materials were characterized through scanning electron microscopy (SEM), Fourier transform infrared spectroscopy (FTIR) and X-ray diffraction (XRD). A number of adsorption parameters were carried out such as adsorbent dose, pH, contact time, initial concentration, ionic strength. And then, adsorption isotherms, kinetics and thermodynamics were also studied. This study has certain reference significance for agricultural waste utilization and sewage treatment.

MATERIALS AND METHODS

1. Chemicals

All chemicals in this work were of analytical grade. MB (chemical formula: $C_{16}H_{18}N_3SCl$, molecular weight: 373.9 g mol^{-1}, solubility in water: 40 g L^{-1}) was purchased from Fuchen Chemical Co., Tianjin, China [26]. The stock solution of MB (1,000 mg L^{-1}) was prepared by dissolving MB powders in distilled water, using a 1,000 mL volumetric flask. The MB working solutions were diluted to the desired concentration by adding distilled water. 1.0 CMC SDS solution: the SDS solution was prepared by adding 2.307 g SDS powder into 1,000 mL distilled water. To adjust the pH, 0.01 mol L^{-1} and 0.1 mol L^{-1} HCl or NaOH solutions were used.

2. Materials Preparation

OA: fresh okara was obtained from Northeast Agricultural University canteen. To remove the impurity, the okara was immersed into tap water for 24 h and washed with distilled water repeatedly. Then, it was dried in the oven at 60 °C until constant weight. The dried okara was powdered, sieved (<0.25 mm), and stored for use.

SOA: the OA was impregnated with 1.0 CMC SDS solution (1,000 mL) for 6 h, and then washed with distilled water to remove residual SDS [27]. Afterward, the sample was dried in the oven at 60 °C until constant weight (SOA) before use.

3. Samples Characterization

The textural properties of samples were determined using surface area and porosity analyzer under the condition of a degassing temperature of 353 K (ASAP2020, USA). The surface morphology was identified by field emission scanning electron microscopy (SEM, ZEISS EVO 60, Germany). And the samples surface functional groups were performed by a Fourier transform infrared spectrometer (FTIR, Nicolet 6700, USA) with the wavenumber range of 4,000-400 cm^{-1}. The structure of samples was obtained from an X-ray diffractometer (XRD, D8 Avance, Bruker, Germany) by using Cu K_α radiation. The scanning range was recorded from 5° to 70° at 3°/min. The point of zero charge (pH_{pzc}) of OA and SOA was determined by the pH drift method [28]. A 0.01 mol L^{-1} NaCl (50 mL) was added into each flask and was adjusted to a pH range 2.0-12.0 using 0.1 mol L^{-1} HCl or NaOH. Then, 0.1 g OA or SOA was put in every flask, the flasks were shaken for 48 h at 25 °C. Lastly, the final pH (pH_f) of the samples was determined. The pH_{pzc} was defined as the point where the curve is determined by pH_i=pH_f.

4. Batch Adsorption Experiments

The adsorption studies were carried out with OA and SOA by batch experiments. The adsorption performance of MB was determined in terms of removal percentage and uptake. A set of batch experiments were investigated from some necessary variables, which included contact time, initial concentration, adsorbent dose, ionic strength and the solution pH. 0.02 g adsorbent and 25 mL MB solution were put in a 50 mL conical flask. The pH of the solutions was kept natural. These flasks were shaken in a shaker at 165 rpm for the required time at 25 °C. The detailed process was conducted by varying the adsorbent dose (0.4-1.2 g L^{-1}), initial MB concentration (25-250 mg L^{-1}), contact time (0-4 h), ionic strength (0.4-4.0 mol L^{-1}), and the solution pH (2.0-12.0). Ten milliliters of the solution was filtered to determine the final MB concentration. All the experiments were determined in triplicates by using a UV-vis spectrophotometer at λ=662 nm (V550, Jasco Co., Tokyo, Japan) and finally taking the average of three operations. The adsorption capacity at equilibrium (q_e, mg g^{-1}) and the removal percentage (R%) were calculated as follows:

$$q_e = \frac{(C_i - C_e) * V}{W} \quad (1)$$

$$R\% = \frac{(C_i - C_e)}{C_i} * 100 \quad (2)$$

where C_i (mg L^{-1}) and C_e (mg L^{-1}) are the initial and equilibrium concentration, respectively, V (L) is the MB volume, and W (g) is the adsorbent dose.

5. Adsorption Kinetics

The pseudo-first-order and pseudo-second-order model were fitted to the kinetics data at different time intervals (0-4 h). These equations follow [29]:

Pseudo-first-order model:

$$\frac{1}{q_t} = \frac{k_1}{q_e t} + \frac{1}{q_e} \quad (3)$$

Pseudo-second-order model:

$$\frac{t}{q_t} = \frac{1}{k_2 q_e^2} + \frac{t}{q_e} \quad (4)$$

where q_e and q_t (mg g^{-1}) are the MB uptake at the equilibrium and t time (min), respectively, k_1 (min^{-1}) and k_2 (g mg^{-1} min^{-1}) are the pseudo-first-order and pseudo-second-order kinetics rate constants,

respectively.

6. Adsorption Isotherms

The experimental equilibrium data was fitted to the Langmuir and Freundlich models at a MB concentration range of 25-600 mg L^{-1}. These formulas are as follows [30]:

$$\text{Langmuir: } \frac{C_e}{q_e} = \frac{C_e}{q_m} + \frac{1}{K_L q_m} \tag{5}$$

$$R_L = \frac{1}{1 + K_L C_i} \tag{6}$$

$$\text{Freundlich: } \ln q_e = \frac{1}{n} \ln C_e + \ln K_F \tag{7}$$

where q_m (mg g^{-1}) and q_e (mg g^{-1}) are the maximum and equilibrium adsorption capacity, respectively. And C_i (mg L^{-1}) and C_e (mg L^{-1}) are the initial and equilibrium concentration, respectively. K_L (L mg^{-1}) is Langmuir constant which is related to the adsorption energy. R_L is the dimensionless separation factor. K_F (L mg^{-1}) and n are the Freundlich constants which are on behalf of adsorption capacity and strength.

7. Error Analysis

To confirm the validity of isotherm and kinetics models, an error analysis (residual sum of squares) was also conducted; expression of the same is given Eq. (8) [31,32]:

$$RSS = \sum_{i=1}^{n} (q_{e,\,i,\,calc} - q_{e,\,i,\,meas})^2 \tag{8}$$

8. Adsorption Thermodynamics

To study the effect of the temperature on the adsorption process and the change of energy, thermodynamic parameters were determined at different temperatures from 295 K to 304 K. Gibbs free energy (ΔG^o), enthalpy (ΔH^o) and entropy (ΔS^o) are determined by the following formulas [33]:

$$\Delta G^o = -RT \ln K_d \tag{9}$$

$$\ln K_d = \frac{\Delta S^o}{R} - \frac{\Delta H^o}{RT} \tag{10}$$

where K_d is the adsorption distribution coefficient, T (K) is the experimental temperature and R (8.314 J mol^{-1} K^{-1}) is the gas constant.

K_d at different temperatures is measured by the intercept of line ln (q_e/C_e) versus q_e.

9. Desorption Experiments

To evaluate the desorption ability of OA and SOA, adsorbents were accurately weighed with a mass of 1 g of 5 copies to perform MB adsorption. After adsorption saturation, the obtained OA and SOA were washed with distilled water repeatedly and dried for further use. And then the MB loaded adsorbents were put in closed glass containers with 100 mL distilled water for each as regenerating solution. After that, all the glass containers were placed in the ultrasonic generator with immersed water and performed under 2 h ultrasonic oscillation [34]. The collected adsorbents were with distilled water and dried to carry out for the next adsorption-desorption cycles for four times. Finally, the MB removal percentage was used to evaluate the desorption ability of OA and SOA.

10. Statistical Analysis

All samples were run in triplicate and the results were averaged. Regression models were performed using SPSS 19.0. The results were presented in a graph using Origin 2017.

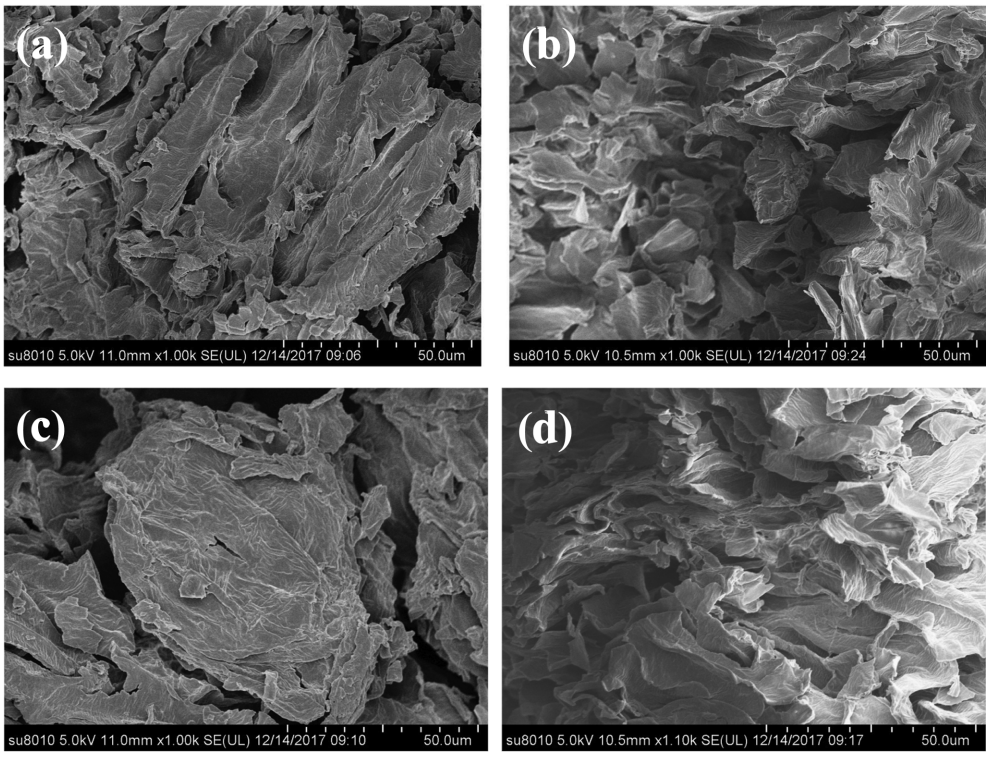

Fig. 1. SEM image (a) OA (b) SOA (c) OA-MB (d) SOA-MB.

RESULTS AND DISCUSSION

1. Characterization of the Materials

The SEM images of OA and SOA at 1,000× magnification are shown in Fig. 1. Both OA and SOA were observed to have numerous holes and folds. Pore characteristics of native materials are presented in Table 2. The BET surface area (1.70 m^2/g), Langmuir surface

Table 2. Pore characteristics of the materials

Indicates	OA	SOA	
BET surface area	1.05	1.70	m^2/g
Langmuir surface area	2.10	2.79	m^2/g
Total pore volume	0.003	0.006	cm^3/g
Average pore diameter	12.93	13.14	nm

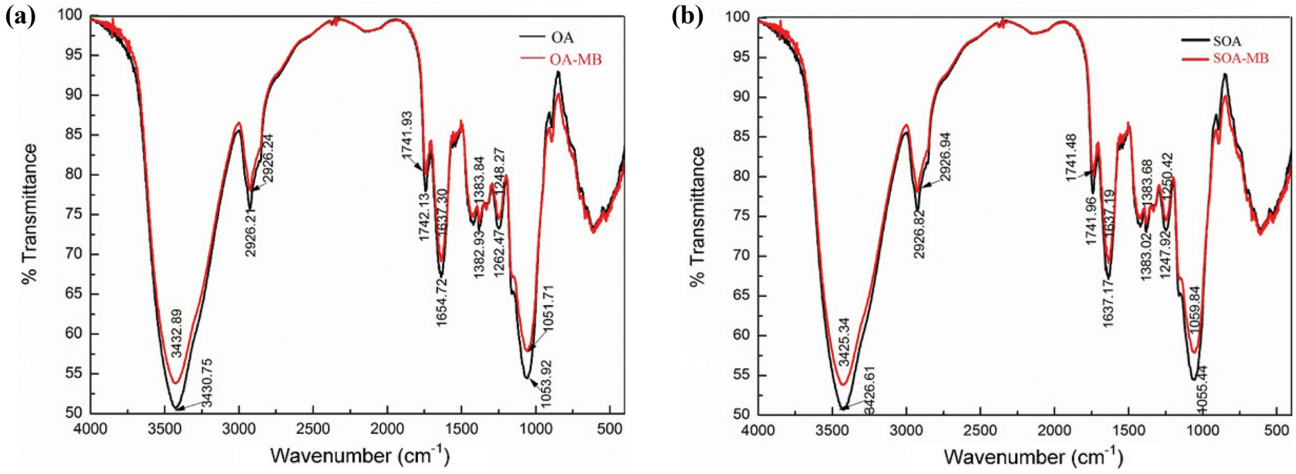

Fig. 2. FTIR spectrums of samples. (a) OA before and after MB adsorption; (b) SOA before and after MB adsorption.

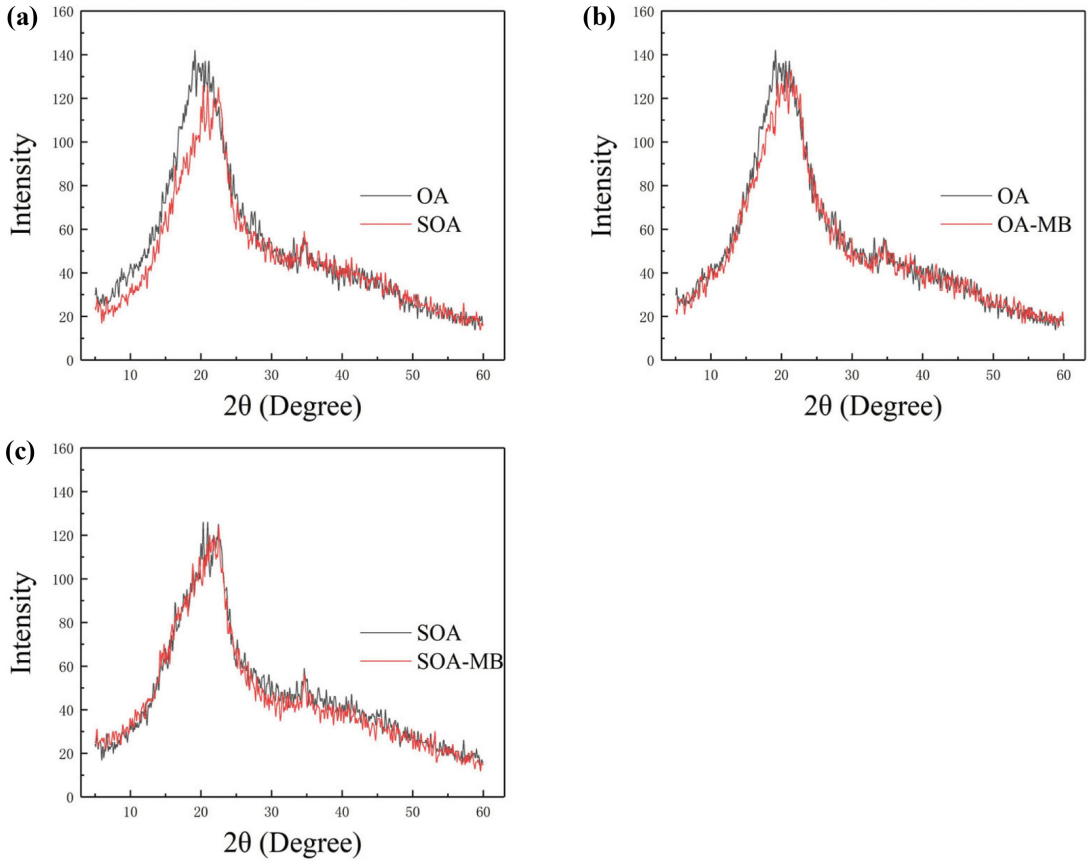

Fig. 3. The XRD patterns of samples. (a) A comparison among two native materials; (b) A comparison between OA and OA-MB; (c) A comparison between SOA and SOA-MB.

area (2.79 m^2/g), total pore volume (0.006 cm^3/g) and average pore diameter (13.14 nm) of SOA were all higher than that of OA, which implies that SOA has more space and surface for adsorption. Collected FTIR spectra for native and MB-loaded materials are shown in Fig. 2. These peaks represent specific functional groups, and the change in wavenumber of peaks indicates participation of corresponding functional groups in the reaction [35]. Comparing the spectral lines of OA and OA-MB (Fig. 2(a)), the peak wavenumbers at 3,430.75 cm^{-1}, 1,654.72 cm^{-1}, 1,262.47 cm^{-1} and 1,053.92 cm^{-1} have changed obviously, which indicates that O-H, C=O, and C-O-C participated in the adsorption. Among them, O-H and C-O-C are characteristic functional groups of cellulose. Comparing the spectral lines of SOA and SOA-MB (Fig. 2(b)), only the wavenumber of C-O-C (1,055.44 cm^{-1}) changed obviously. This indicates that after loading SDS, cellulose was still involved in adsorption, while other functions were not active. Comparing the O-H and C-

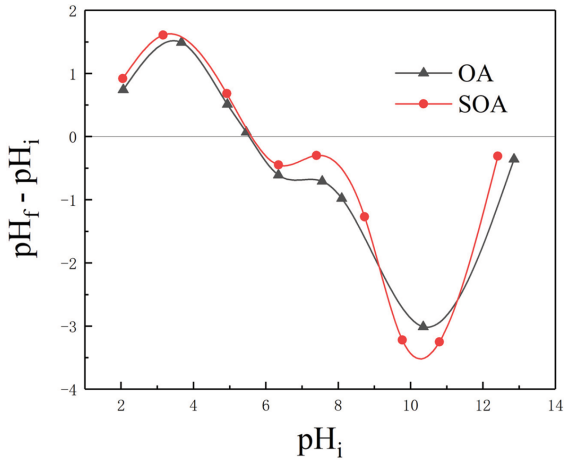

Fig. 4. The pH_{pzc} of OA and SOA.

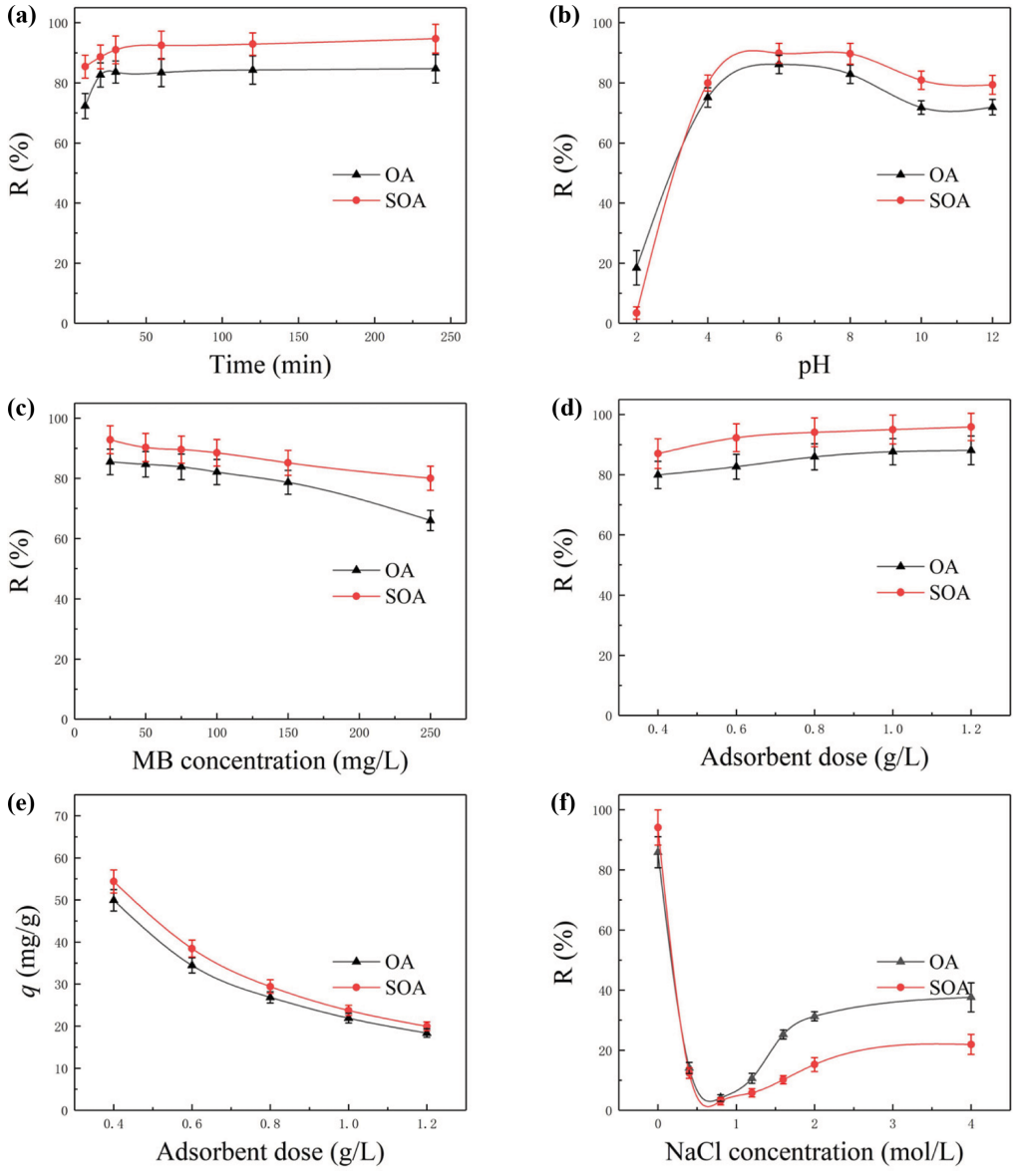

Fig. 5. Influencing factors of adsorption efficiency.

O-C characteristic peaks of OA and SOA, the change of wave number can be found, which indicates that SDS was mainly loaded on cellulose.

The XRD patterns of OA and SOA are shown in Fig. 3. The spectrum corresponds to the characteristic XRD pattern of cellulose [36,37], which indicates the intensive diffraction peaks at 2θ values of about 22°. It should be pointed out that no new peak appeared, from which can be inferred the adsorbents still held the original structure though after SDS treatment. The peaks of SOA and SOA-MB almost coincide, which indicates that the cellulose content of SOA was more stable.

The point of zero charge (pH_{pzc}), where net charge of adsorbent surface is zero, is closely related to the electrostatic forces of adsorbent and adsorbate. Thus, when the solution of $pH<pH_{pzc}$, the adsorbent surface is positively charged, while the adsorbent has negatively charged surface at $pH>pH_{pzc}$. According to Fig. 4, the pH_{pzc} of OA and SOA were 5.5 and 5.7, respectively.

2. Factors Affecting Adsorption

2-1. Effect of Contact Time

The influence of contact time is illustrated in Fig. 5(a), which determines the reaction efficiency directly. It was observed that the adsorption process was divided into two steps. In the first 30 min, the removal percentage of OA and SOA rose rapidly to 83.62% and 91.70%, respectively. At the next step, the growing tendency went slowly until achieving the maximal removal percentage with the time range of 30-240 min. These results were because of the available adsorption sites initially; after that, the removal percentage increased slowly with the saturation of the active sites during the adsorption [38]. To reach the equilibrium state thoroughly, 2 h was selected as the optimum for the adsorption of MB on OA and SOA. At all-time points, the R value of SOA was always higher than that of OA.

2-2. Effect of pH

The effect of pH on the adsorption of MB was studied because pH is one of the most important factors during adsorption [39]. Results are shown in Fig. 5(b). The R values of OA and SOA were similar with the initial pH of solution. Except for pH 2, the R value of SOA is higher than that of OA. The removal percentage increased with the increasing of pH value until at pH 6.0. Then, the trends decreased slowly until a plateau at higher pH ($8.0<pH<12.0$). This was primarily due to the excess H^+ ions at lower pH had a competition with cationic MB molecules via electrostatic repulsion. However, at higher pH, OA and SOA with negative charges were in favor of MB adsorption through electrostatic attraction; consequently, the removal percentage increased. This inference can also be proved by the point of zero charge (pH_{pzc}). As shown in Fig. 4, the pH_{pzc} of OA and SOA was 5.5 and 5.7, respectively. When $pH>pH_{pzc}$, OA and SOA charged negatively and facilitated the MB adsorption, whereas the condition was opposite in the case of $pH<pH_{pzc}$.

2-3. Effect of Initial MB Concentration

As presented in Fig. 5(c), the removal percentage decreased from 85.91% to 66.03% for OA and 92.92% to 80.07% for SOA, at the initial concentration range between 25 mg L^{-1} and 250 mg L^{-1}. This fact was attributed to the limited available adsorption sites at a fixed adsorbent dose. Though at higher concentration, the adsorption sites went saturated, which restricted the adsorption process [40].

2-4. Effect of Adsorbent Dose

The effects of OA and SOA dose on the removal of MB are represented in Fig. 5(d) and (e). The adsorption capacity of SOA was stronger than that of OA for all doses. The MB removal percentage increased and adsorption uptake decreased with the increasing of biosorbent dose. The removal percentage of OA and SOA increased from 79.91% to 88.10% and 87.03% to 95.87%, respectively, with a range of 0.4-1.2 g L^{-1} of the biosorbent dose. This is due to more available adsorption sites at higher amount of the biosorbent. At the same time, the q values decreased from 49.91 mg g^{-1} to 18.42 mg g^{-1} for OA and 54.40 mg g^{-1} to 20.01 mg g^{-1} for SOA. This can be ascribed to the unsaturation of adsorbent sites during the adsorption [41]. Nevertheless, in the light of the huge yield of okara annually, 0.8 g L^{-1} of adsorbent dose was the optimal choice.

2-5. Effect of Ionic Strength

The effect of NaCl on the adsorption of MB onto OA and SOA was investigated (Fig. 5(f)). The removal percentage of OA and SOA decreased from 85.90% to 4.12% and 94.11% to 3.04%, respectively, at lower NaCl additions (0-0.8 mol L^{-1}). This can be ascribed to the competitive adsorption between the excess salt ions and cationic MB molecules, which inhibited the adsorption process [42]. Then, the removal percentage increased slightly when NaCl additions increased. Since at higher NaCl addition (0.8-4.0 mol L^{-1}), the concentration of salt ions in the solution increased, the number of anions and cations in the solution increased correspondingly, which made the double layer structure formed by electrostatic action extruded, thus increasing the contact probability of dye molecules with the surface of adsorbents. At the same time, the increase of salt ion concentration was helpful to the formation of dye dimer, which was beneficial to the adsorption of dye [43]. NaCl inhibited SOA adsorption more strongly than OA, which may be related to the high Na salt content of SOA itself.

3. Adsorption Kinetics

Kinetics study is applied to describe the adsorption rate and mechanism, which is extremely necessary in real work [44]. The experimental data was investigated to match with the pseudo-first-order

Table 3. Kinetics parameters of pseudo-first-order and pseudo-second-order models on OA and SOA at 22 °C

Samples	Pseudo-first-order model				Pseudo-second-order model				Experiment
	k_1 (min^{-1})	Calculated q_e (mg g^{-1})	R^2	RSS	k_2 (g mg^{-1} min^{-1})	Calculated q_e (mg g^{-1})	R^2	RSS	q_e (mg g^{-1})
OA	0.0222	2.07	0.9997	3.62×10^{-3}	0.0340	26.80	1.0000	1.13×10^{-3}	26.71
SOA	0.0344	4.02	0.9969	1.21×10^{-1}	0.0214	29.76	0.9999	2.69×10^{-3}	29.60

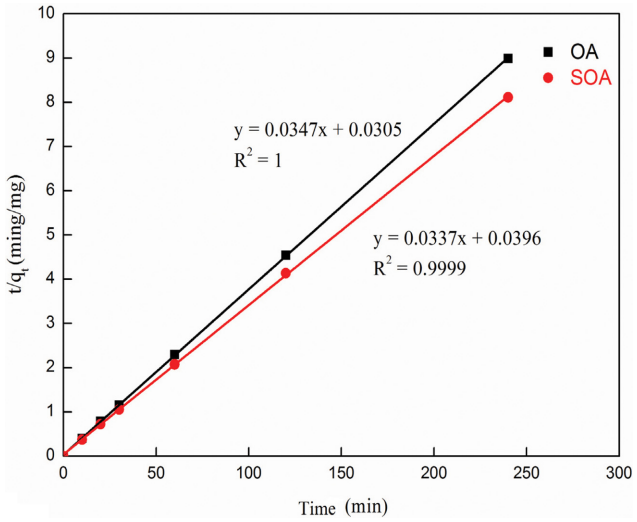

Fig. 6. Pseudo-second-order kinetic model of MB onto OA and SOA (C_i=25 mg L^{-1}, adsorbent dose=0.8 g L^{-1}, pH 5.6 and 25 °C).

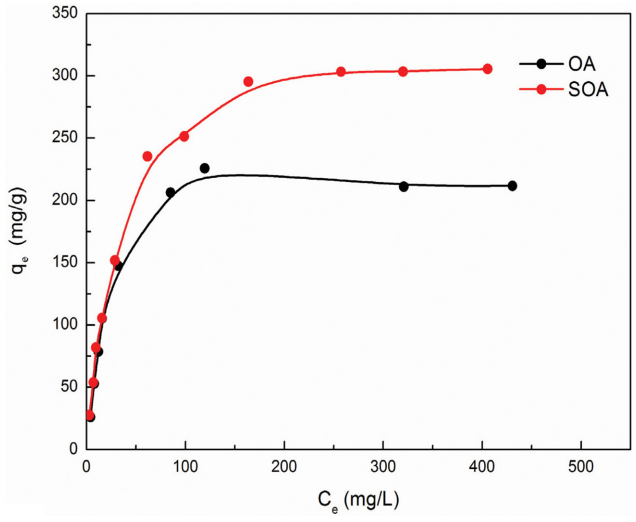

Fig. 7. Adsorption isotherms of MB on OA and SOA (C_i=25-600 mg L^{-1}, adsorbent dose=0.8 g L^{-1}, shaking time 24 h, pH 5.6 and 25 °C).

and pseudo-second-order kinetics models. The detailed parameters calculated by kinetics equations are in Table 3. The R^2 of pseudo-second-order (1.0000 for OA and 0.9999 for SOA) was higher than pseudo-first-order (0.9997 for OA and 0.9969 for SOA) both OA and SOA; in the meantime, the calculated q_e was highly near to the experiment q_e. And RSS also confirmed the feasibility of the pseudo-second-order model. Taking account of these two factors, the adsorption of MB onto OA and SOA followed the pseudo-second-order model accurately. The well-fitted pseudo-second-order models of OA and SOA are demonstrated in Fig. 6. The fact indicates that the rate of the adsorption process is mainly controlled by chemisorption [45].

4. Adsorption Isotherms

Adsorption isotherms are essential to describing the interaction of adsorbent-adsorbate [46]. Langmuir isotherm model assumes the adsorption is monolayer and the adsorbent surface is homogeneous [47]. The Freundlich isotherm model is used to perform multilayer adsorption onto the heterogeneous adsorbent surface [48].

The q_e at various MB concentration (25-600 mg L^{-1}) is shown in Fig. 7. It can be observed that the adsorption capacity of OA and SOA increased until at an equilibrium state with increasing concentration. The results above were fitted with Langmuir and Freundlich models and the detailed parameters are revealed in Table 4. It is clear that the Langmuir model matches better than Freundlich model with higher correlation coefficient (R^2). The fitted Langmuir models of OA and SOA are demonstrated in Fig. 8(a) and (b). The q_m of OA and SOA were 238.10 mg g^{-1} and 334.83 mg g^{-1}, respectively, close to the equilibrium adsorption capacity. RSS also confirmed the feasibility of the Langmuir model. Therefore, the adsorption of MB onto OA and SOA is monolayer. And the R_L values were all between 0 and 1, which indicates OA and SOA are in favor of the MB adsorption. It is also evident that the values of

Table 4. Isotherm parameters of Langmuir and Freundlich models on OA and SOA at 22 °C

Samples	Langmuir model					Freundlich model			
	q_m (mg g^{-1})	K_L (L mg^{-1})	R_L	R^2	RSS	K_F (L mg^{-1})	n	R^2	RSS
OA	238.10	0.05	0.03-0.44	0.9877	426.65	24.85	2.40	0.8232	14,046.81
SOA	334.83	0.03	0.59-0.97	0.9962	392.09	21.06	1.88	0.9433	19,563.31

Table 5. Thermodynamic parameters for adsorption of MB on OA and SOA

Samples	T (K)	K_d	ΔH^o (J mol^{-1})	ΔS^o (J mol^{-1})	ΔG^o (J mol^{-1})
OA	295	2.9664	−26,457	79	−2,667
	301	2.4469			−2,239
	304	2.1428			−1,926
SOA	295	2.8115	−26,298	−81	−2,535
	301	2.5173			−2,297
	304	2.1175			−1,896

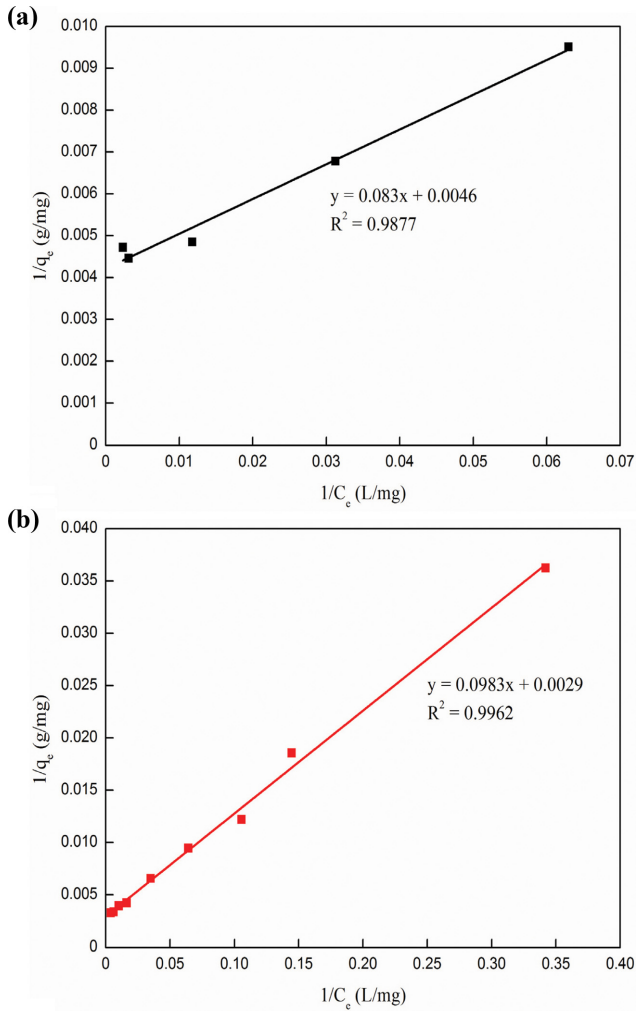

Fig. 8. Linear Langmuir plots of MB adsorption on OA (a) and SOA (b).

n are favorable for adsorption with the range of 1<n<10.

5. Adsorption Thermodynamics

Table 5 lists the detailed thermodynamic parameters of OA and SOA at various temperatures. The ΔG^o values of OA were −2,667 J mol^{-1}, −2,239 J mol^{-1} and −1,926 J mol^{-1}, respectively, while of SOA were −2,535 J mol^{-1}, −2,297 J mol^{-1} and −1,896 J mol^{-1}, respectively. The negative ΔG^o reveals the spontaneity and feasibility of adsorption. The ΔG^o decreased with increasing temperature, which suggests the exothermal nature. Similar evidence was confirmed by the negative ΔH^o (−26,457 J mol^{-1} for OA and −26,298 J mol^{-1} for SOA). Lastly, the values of ΔS^o were 79 J mol^{-1} for OA and −81 J mol^{-1} for SOA, respectively.

6. Desorption and Reuse of Adsorbents

The desorption and reusability of adsorbents are used to determine the adsorption capacity in practical application [49]. As displayed in Fig. 9, after 2 h ultrasonic oscillation, the removal percentages decreased from 85.91% to 72.91% for OA and 94.11% to 73.61% for SOA, respectively. After three adsorption-desorption cycles, the removal percentages of OA and SOA were eventually 64.05% and 68.79%, respectively. It is due to the damage of adsorbents structure under ultrasonic oscillation, which leads to the decline of removal percentage directly. Nevertheless, after several cycles, OA and SOA still performed a showed better adsorption behavior. Consequently, OA and SOA exhibit a prominent application in real wastewater treatment.

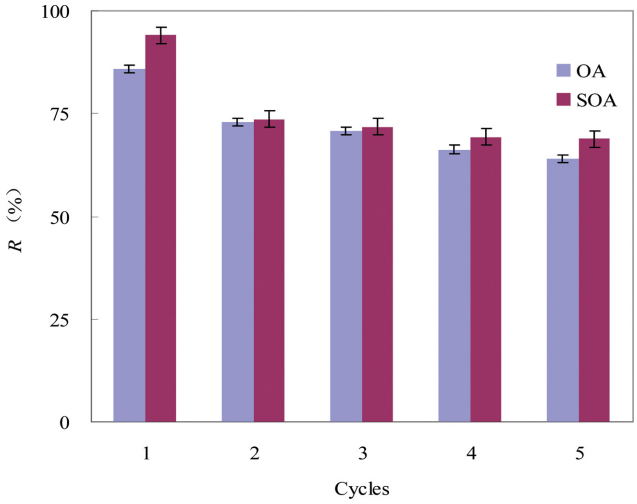

Fig. 9. Effect of pH on the adsorption of MB on OA and SOA (C_i= 25 mg L^{-1}, adsorbent dose=0.8 g L^{-1}, shaking time 2 h and 25 °C).

In summary, SDS modification can increase the pore size and specific surface area of OA. SDS may be loaded on cellulose mainly by interaction with corresponding functional groups. In the process of adsorption, the initial structure of the two materials is basically maintained, the functional groups involved in the chemical reaction are less, MB is captured (or up taken) mainly by electrostatic adsorption. The modified material is more stable and not easy to lose cellulose, which is helpful to reduce the secondary pollution caused by dissolved organic matter. Under a variety of environmental conditions, SOA shows better adsorption performance than raw materials. But due to the influence of loading salt, the adsorption performance of the modified material is not as good as that of the raw material in high salt solution. The results of this study mean that SDS may be more effective on the modification of agricultural wastes, which can be used as a reference for other materials. Moreover, the effect of salt is a problem that needs to be paid attention to.

7. Cost Analysis

In recent years, due to the high cost of activated carbon used as an adsorbent, more and more agricultural wastes have been explored and applied as biosorbent in the field of adsorbing dye wastewater to develop the resource utilization of agricultural wastes. Among them, treatment of rice husks with sodium carbonate to adsorb malachite green [50], adsorption with peanut husks to remove hazardous dyes from water [51], and removal of bright green dyes from water using modified bamboo have fully realized the reuse value of agricultural wastes [52].

The soybean residue used in this study is the remaining waste during the production of soy products. Due to their huge production, about 20 million tons per year [16], leading to the disposal of soybean residue waste which becomes a significant environmental

Table 6. The adsorption capacity of other adsorbents for MB

Adsorbents	Maximum adsorption capacity (mg g^{-1})	Ref.
Sepiolite	57.38	[53]
Pyrolysed sewage sludge	92.60	[54]
NaOH modified rubber tire	163.12	[55]
Coffee waste	180.70	[56]
Rice straw based carbons	200.00	[57]
Activated furniture (850 °C)	200.00	[58]
OA	238.10	This study
SOA	334.83	This study

problem. Compared with the similarly previous studies (as shown in Table 6), OA and SOA exhibit a higher adsorption capacity than other materials, which indicates that the adsorbent materials and modification methods selected in this study have a good prospect. Meanwhile, the soybean residue also contains a large amount of nutrients, the direct discarding of which will cause a serious waste of resources [17]. So it is very necessary to use the soybean residues to remove dye wastewater, which can not only replace activated carbon to complete the dye wastewater adsorption work to reduce economic cost, but also alleviate the environmental problems of agricultural wastes, and have great economic and resource benefits.

8. Adsorption Mechanism

The adsorption of MB on adsorbents may include several steps, such as film diffusion, intraparticle diffusion and adsorption on the surface. However, the pseudo-first-order and pseudo-second-order models cannot describe the diffusion mechanism. Therefore, intraparticle and external diffusion models were determined for the adsorption mechanism. These equations are expressed as follows [59]:

Intraparticle diffusion model:

$$q_t = k_{id} t^{1/2} + C \quad (11)$$

External diffusion model:

$$\ln\left(1 - \frac{q_t}{q_e}\right) = -k_{fd} t \quad (12)$$

where k_{id} (mg g^{-1} $min^{-1/2}$) and k_{fd} (t^{-1}) are the intraparticle and external diffusion rate constants, respectively, and C (mg g^{-1}) is a constant which is in relation with boundary layer thickness.

The linear fitting images of intraparticle and external diffusion on OA and SOA are in Fig. 10 and Fig. 11. The specifically calculated parameters are reported in Table 7. The R^2 of intraparticle diffusion model was lower than that of external diffusion model, and the lines did not go through the origin. These facts explain that intraparticle diffusion is not the only rate-limiting procedure. And then, the lines of external diffusion did not pass through the origin likewise. It shows the adsorption process of OA and SOA is primarily commanded by external diffusion [60].

At the same time, from the results of the SEM diagram, the surface of the two adsorbents does not show obvious micropore structure, but the adsorption sites are provided by more folds. Next, by observing the comparison of the FTIR diagram of the adsorption of MB by OA and SOA, it was found that the adsorbents contained a large number of oxygen-containing functional groups, all of which were negatively charged. The adsorption effect was achieved by com-

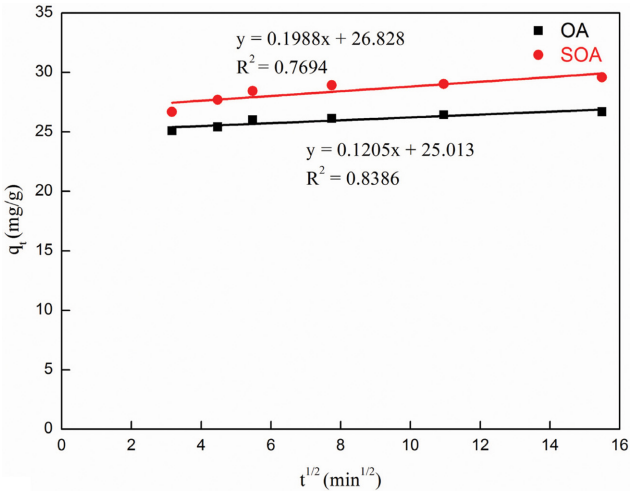

Fig. 10. Intraparticle diffusion model for adsorption of MB on OA and SOA (C_i=25 mg L^{-1}, adsorbent dose=0.8 g L^{-1}, pH 5.6 and 25 °C).

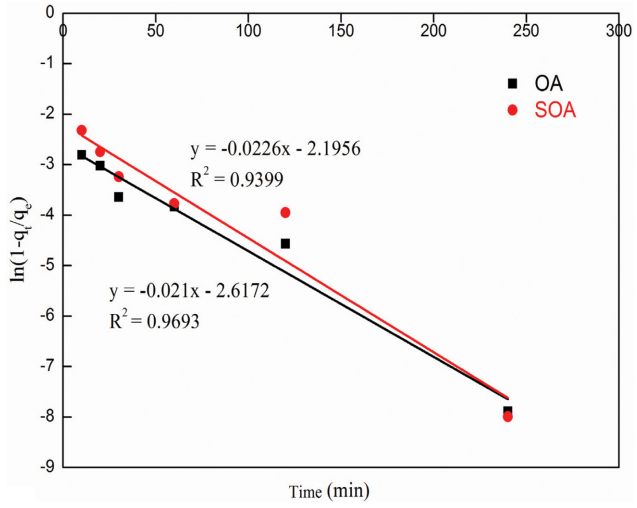

Fig. 11. External diffusion model for adsorption of MB on OA and SOA (C_i=25 mg L^{-1}, adsorbent dose=0.8 g L^{-1}, pH 5.6 and 25 °C).

Table 7. Parameters of the intraparticle and external diffusion models for MB adsorption on OA and SOA at 22 °C

Samples	Intraparticle diffusion model			External diffusion model	
	k_{id} (mg g^{-1} $min^{-1/2}$)	C (mg g^{-1})	R^2	k_{fd} (min^{-1})	R^2
OA	0.1205	25.013	0.8386	0.0210	0.9693
SOA	0.1988	26.828	0.7694	0.0226	0.9399

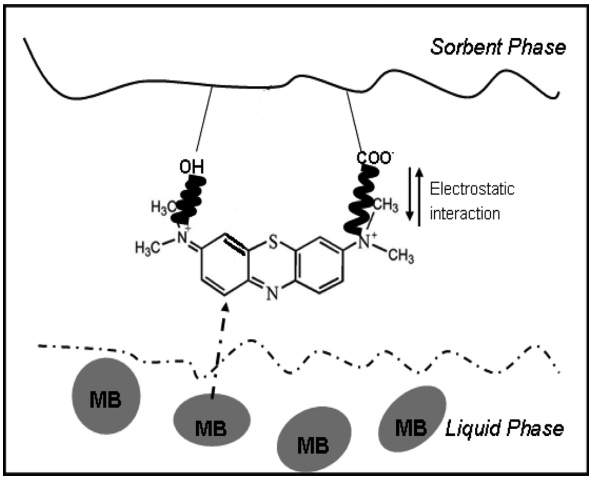

Fig. 12. The mechanism of MB adsorption on OA and SOA.

bining the cationic chromogenic group N^+ in MB with electrostatic attraction. Before and after adsorption, the main functional groups were hydroxyl group (O-H) and carbonyl group (C=O). In the study, after being modified by SDS, the surface of SOA carried more anion groups, which further enhanced the electrostatic attraction between adsorbents and adsorbents, so that the adsorption effect was enhanced and the effect of modification was obtained. At the same time, according to the influence of pH value of solution on the experimental results, it can be predicted that the change of pH value of solution has a very significant effect on the adsorption effect. It is shown from the side that electrostatic action is the important role of adsorbents OA and SOA on adsorption of adsorbents; the detailed adsorption mechanism diagram is shown in Fig. 12. Zhu et al. used citric acid modified soybean straw to adsorb copper ions in water solution [61]. Through citric acid modification, the surface carried more -COOH groups, and when the solution pH was higher than 3.0, this group appeared in the form of COO- in the solution, which enhanced the electrostatic interaction with copper ions. Therefore, the electrostatic attraction and hydrogen bond between the adsorbent and MB molecules were the main forces in the adsorption process. Yao et al. used tea waste-nano Fe_3O_4 composite adsorbent to adsorb MB in water solution [62]. According to the kinetics and the results of FTIR and XPS analysis, it was found that there was strong electrostatic interaction between the functional groups (O-H) and (C-N) and MB molecules on the surface of the complex adsorbents.

CONCLUSIONS

Considering that the optimal dose of adsorbents was 0.8 g L^{-1} and the equilibrium time was 2 h, the removal percentage decreased with increasing initial MB concentration, while the adsorption process was favored in alkaline conditions. Meanwhile, in the presence of salt, the removal percentage decreased sharply, but rose slightly at higher salt addition. The Langmuir isotherm fitted well with the equilibrium data, which indicated monolayer adsorption, and the calculated maximum adsorption capacity was 238.10 mg g^{-1} for OA and 334.83 mg g^{-1} for SOA, respectively. The kinetics data was the most suitable for the pseudo-second-order model, which signified the rate-limiting step was mainly commanded by chemisorption. Additionally, the fitting results of intraparticle and external diffusion models implied the leading role of external diffusion during the adsorption. Thermodynamic parameters (ΔH_0, ΔG_0 and ΔS_0 revealed the exothermal, spontaneous and feasible adsorption reaction. As expected, SDS enhanced the ability of MB adsorption by OA and made the material more stable. The SOA would be an effective, low-cost and environmentally friendly agricultural waste biosorbent for the removal of MB in wastewater.

ACKNOWLEDGEMENTS

The authors would like to thank the editors and anonymous reviewers for their valuable comments and suggestions on this paper.

FUNDING

This work was supported by the National Key R&D Program of China (2017YFD0200104, 2016YFD0300909).

REFERENCES

1. W. Li, B. Mu and Y. Yang, *Bioresour. Technol.*, **277**, 157 (2019).
2. P. Wang, M. Cao, C. Wang, Y. Ao, J. Hou and J. Qian, *Appl. Surf. Sci.*, **290**, 116 (2014).
3. S. Shakoor and A. Nasar, *J. Taiwan Inst. Chem. E.*, **66**, 63 (2016).
4. C. Zhou, Q. Wu, T. Lei and I. I. Negulescu, *Chem. Eng. J.*, **251**, 17 (2014).
5. E. Lacasa, P. Canizares, F. C. Walsh, M. A. Rodrigo and C. Ponce-de-Leon, *Electrochim. Acta*, **308**, 45 (2019).
6. M. Moztahida and D. S. Lee, *J. Hazard. Mater.*, **400**, 123314 (2020).
7. S. Sahu, S. Pahi, S. Tripathy, S. K. Singh, A. Behera, U. K. Sahu and R. K. Patel, *J. Mol. Liq.*, **315**, 113743 (2020).
8. Y. Jiang, Y. Qin, T. Yu and S. Lin, *Chin. Chem. Lett.*, **32**, 1823 (2021).
9. Y. Dai, K. Zhang, X. Meng, J. Li, X. Guan, Q. Sun, Y. Sun, W. Wang, M. Lin, M. Liu, S. Yang, Y. Chen, F. Gao, X. Zhang and Z. Liu, *Chemosphere*, **215**, 163 (2019).
10. V. Narayanaswamy, S. Alaabed and I. M. Obaidat, *Mater. Today: Proceedings*, **28**, 1078 (2020).

11. L. Wang, Y. Guo, B. Zou, C. Rong, X. Ma, Y. Qu, Y. Li and Z. Wang, *Bioresour. Technol.*, **102**, 1947 (2011).
12. Y. Dai, W. Wang, L. Lu, L. Yan and D. Yu, *J. Clean. Prod.*, **257**, 120573 (2020).
13. Y. O. Al-Ghamdi, M. Jabli, R. Soury and S. A. Khan, *Polymers*, **12**, 2539 (2020).
14. K. Y. Foo and B. H. Hameed, *Chem. Eng. J.*, **180**, 66 (2012).
15. M. T. Yagub, T. K. Sen, S. Afroze and H. M. Ang, *Adv. Colloid Interface Sci.*, **209**, 172 (2014).
16. A. Asfaram, M. Ghaedi and K. Dashtian, *ACS Sustain. Chem. Eng.*, **6**, 4549 (2018).
17. B. Li, M. Qiao and F. Lu, *Food Rev. Int.*, **28**, 231 (2012).
18. S. Mosleh, M. R. Rahimi and M. Ghaedi, *RSC Adv.*, **6**, 21 (2016).
19. J. Gao, J. Wang, C. Yang, S. Wang and Y. Peng, *Chem. Eng. J.*, **171**, 967 (2011).
20. L. Ye, X. Bai and H. Chen, *J. Southwest China Normal Univ. (Nat. Sci. Ed.)*, **4**, 83 (2014).
21. Y. Park, G. A. Ayoko and R. L. Frost, *J. Colloid Interface Sci.*, **354**, 292 (2011).
22. Y. Zhang, G. Huang, C. An, X. Xin, X. Liu, M. Raman, Y. Yao, W. Wang and M. Doble, *Sci. Total Environ.*, **595**, 723 (2017).
23. I. Fatimah, I. Sahroni, M. S. E. Dahlyani, A. M. N. Oktaviyani and R. Nurillahi, *Mater. Today: Proceedings*, **44**, 3211 (2021).
24. Y. Kuang, X. Zhang and S. Zhou, *Water*, **12**, 587 (2020).
25. S. Yamaguchi, S. Minbuta and K. Matsui, *Langmuir*, **36**, 4592 (2020).
26. M. A. Islam, S. Sabar, A. Benhouria, W. A. Khanday, M. Asif and B. H. Hameed, *J. Taiwan Inst. Chem. E.*, **74**, 96 (2017).
27. T. Liu, R. Guo, M. Shen and W. Yu, *Acta Phys.-Chim. Sin.*, **27**, 297 (1996).
28. L. Eskandarian, E. Pajootan and M. Arami, *Ind. Eng. Chem. Res.*, **53**, 14841 (2014).
29. S. Mosleh, *Ultrason. Sonochem.*, **40**, 601 (2018).
30. M. Auta and B. H. Hameed, *Chem. Engr. J.*, **198-199**, 219 (2012).
31. F. Batool, J. Akbar, S. Iqbal, S. Noreen and S. N. A. Bukhari, *Bioinorg. Chem. Appl.*, **11**, 1 (2018).
32. L. S. Chan, W. H. Cheung, S. J. Allen and G. McKay, *Chin. J. Chem. Eng.*, **535**, 20 (2012).
33. C. Saucier, M. A. Adebayo, E. C. Lima, R. Cataluna, P. S. Thue, L. D. Prola, M. J. Puchana-Rosero, F. M. Machado, F. A. Pavan and G. L. Dotto, *J. Hazard. Mater.*, **289**, 18 (2015).
34. S. Mosleh, M. R. Rahimi and M. Ghaedi, *RSC Adv.*, **6**, 63667 (2016).
35. S. F. Weng. *Fourier transform infrared spectroscopy analysis*, 2nd Ed. Chemical Industry, Beijing (2010).
36. X. J. Hu, L. L. Yan, H. Gu, T. T. Zang, Y. Jin and J. J. Qu, *Korean J. Chem. Eng.*, **31**, 1911 (2014).
37. X. Liu, X. Bai, L. Dong, J. Liang, Y. Jin, Y. Wei, Y. Li, S. Huang and J. Qu, *J. Clean. Prod.*, **200**, 1 (2018).
38. F. A. Pavan, E. C. Lima, S. L. Dias and A. C. Mazzocato, *J. Hazard. Mater.*, **150**, 703 (2008).
39. Y. Xia, T. Li, J. Chen and C. Cai, *Synth. Met.*, **175**, 163 (2013).
40. M. S. Sajab, C. H. Chia, S. Zakaria and P. S. Khiew, *Bioresour. Technol.*, **128**, 571 (2013).
41. Q. Yue, W. Wang, B. Gao, X. Xu, J. Zhang and L. Qian, *Water Environ. Res.*, **82**, 374 (2010).
42. U. Guyo, T. Makawa, M. Moyo, T. Nharingo, B. C. Nyamunda and T. Mugadza, *J. Environ. Chem. Eng.*, **3**, 2472 (2015).
43. X. Wang, L. Xia, W. Zheng and K. Tan, *Chin. J. Process Eng.*, **10**, 1084 (2011).
44. N. Y. Mezenner and A. Bensmaili, *Chem. Eng. J.*, **147**, 87 (2009).
45. L. Cui, Y. Wang, L. Gao, L. Hu, L. Yan, Q. Wei and B. Du, *Chem. Eng. J.*, **281**, 1 (2015).
46. A. A. EI-Bindary, A. Z. EI-Sonbati, A. A. AI-Sarawy, K. S. Mohamed and M. A. Farid, *J. Mol. Liq.*, **199**, 71 (2014).
47. I. Langmuir, *J. of the Franklin I.*, **183**, 102 (1917).
48. H. Deng, L. Yang, G. Tao and J. Dai, *J. Hazard. Mater.*, **166**, 1514 (2009).
49. M. Jain, V. K. Garg and K. Kadirvelu, *Bioresour. Technol.*, **129**, 242 (2013).
50. B. Kumar and U. Kumar, *Korean J. Chem. Eng.*, **32**, 1655 (2015).
51. A. Herbert, U. Kumar and P. Janardhan, *Water Environ. Res.*, **93**, 1032 (2021).
52. N. Laskar and U. Kumar, *Inter. J. Environ. Sci. Technol.*, **16**, 1649 (2019).
53. F. Lian, B. Xing and L. Zhu, *J. Colloid Interface Sci.*, **360**, 725 (2011).
54. S. Mosleh, M. R. Rahimi and M. Ghaed, *Chem. Eng. Process*, **114**, 24 (2017).
55. Z. Aksu, *Process Biochem.*, **40**, 997 (2005).
56. C. Liu, Z. Tang, Y. Chen, S. Su and W. Jiang, *Bioresour. Technol.*, **101**, 1097 (2010).
57. Y. Yao, F. Xu, M. Chen, Z. Xu and Z. Zhu, *Bioresour. Technol.*, **101**, 3040 (2010).
58. K. A. Krishnan and A. Haridas, *J. Hazard. Mater.*, **152**, 527 (2008).
59. A. Roy, S. Chakraborty, S. P. Kundu, B. Adhikari and S. B. Majumder, *Ind. Eng. Chem. Res.*, **51**, 12095 (2016).
60. M. H. Kalavathy, T. Karthikeyan, S. Rajgopal and L. R. Miranda, *J. Colloid Interf. Sci.*, **292**, 354 (2005).
61. B. Zhu, T. Fan and D. Zhang, *J. Hazard. Mater.*, **153**, 300 (2008).
62. S. Yao, M. Zhang and L. Li, *J. Environ. Sci.*, **37**, 96 (2018).